JOURNAL OF COMPUTATIONAL PHYSICS 122, 13–24 (1995)

Complex Mapped Matrix Methods in Hydrodynamic Stability Problems

ANDREW W. GILL* AND G. E. SNEDDON

Department of Mathematics and Statistics, James Cook University, Townsville 4811, Australia

Received October 5, 1993; revised April 3, 1995

The ordinary differential equations governing the linear stability of inviscid flows contain singularities at real or complex points called critical latitudes, which degrade the accuracy of standard numerical schemes. However, the use of a complex mapping prior to the numerical attack offers some respite. This mapping shifts the computational domain to a contour in the complex plane to avoid the critical latitudes. Both quadratic and cubic complex maps are considered in some detail. An analytic result for choosing the optimum quadratic complex map in the case of a single critical latitude is presented. Numerical results are given for two test problems and a barotropic vortex model. A comparison is made between methods with and without these mappings. The results show that the use of complex maps can lead to remarkably accurate solutions.

1. INTRODUCTION

Hydrodynamic stability calculations often involve the numerical solution of singular differential equations. For example, the linear analysis of inviscid flows results in ordinary differential equations possessing singularities, called critical latitudes, whenever the basic flow matches the wavespeed of the perturbations. For unstable modes these singularities will be complex, but for neutral curve calculations, where the wavespeed is real, they will lie on the computational domain. Excellent reviews of the inviscid theory of hydrodynamic stability [1, 2] indicate the importance of these critical latitudes for the understanding of fluid motion (for example, in meteorology and oceanography), as well as discussing various computational issues. Another example containing real critical latitudes is the Sturm–Liouville problems of the fourth kind [3, 4] which have poles on the interior of the interval. Further examples of singular differential equations are reviewed in [5].

The majority of numerical methods for solving these types of problems are either matrix or shooting methods [3, 6–10]. Matrix methods (including finite difference and pseudospectral methods) solve the eigenvalue problem by approximating it with a finite matrix eigenvalue problem, while shooting methods (e.g., Runge–Kutta or predictor–corrector methods) iterate from an initial guess at the eigenvalue and use a numerical root finder to converge to the answer. However, all of these methods are sensitive to the location of the critical latitudes [3]. For critical latitudes near the computational domain, greater resolution is required to resolve the singularities accurately, resulting in a larger matrix or smaller stepsize, depending on the method used. When the critical latitudes are real, alternative methods of solution must be found.

Matrix methods are generally preferred over shooting methods in solving hydrodynamic stability problems for a number of reasons. First the differential equations are not self-adjoint and so iterative methods have the risk of missing modes of instability. Matrix methods, using the QR algorithm to calculate the matrix eigenvalues, are more robust and will miss a mode only if the resolution is too coarse to resolve that mode's oscillations. Second, matrix methods do not require initial guesses to the eigenvalues, and, finally, they return approximations to more than just one eigenvalue.

Pseudospectral methods are more attractive than finite differences due to the promise of spectral accuracy [11]. That is, the pseudospectral errors decrease faster than any finite power of $1/N$, where N is the number of trial functions. However, pseudospectral methods are particularly sensitive to critical latitudes and their proximity to the computational domain. Recent work [12] on the stability of barotropic vortices compared a pseudospectral method with a second-order finite difference method. It was found that both fared equally badly near the upper limit of unstable wavenumbers where the wavespeed and, therefore, a critical latitude, approach the real axis.

Boyd [3] suggested a remedy for this problem by the use of a complex map. Although motivated originally by pseudospectral methods, the complex map can equally be applied to finite difference and shooting methods [13–15]. Essentially, the problem is solved on a contour in the complex plane chosen to avoid the critical latitudes and their branch cuts and thereby to accelerate convergence. Similar complex mapping techniques have also been used to calculate certain integrals arising in physics [16].

The use of maps in solving differential equations numerically

* Now at the Department of Applied Mathematics, University of Adelaide, 5005, Australia.

0021-9991/95 $12.00

is not new. For example, in [17] semi-infinite and infinite intervals have been mapped to $[-1, 1]$ so that polynomial methods could be applied. These techniques have also been used by Boyd [18, 19]. Also problems with regions of rapid variation or boundary layers benefit from maps which increase the resolution where the gradients are large. Recent examples include acoustic wave propagation in discontinuous media [20] and reaction–diffusion problems [21]. However, these mappings are real-valued and cannot deal with real critical latitudes. The complex maps of Boyd [3] can.

There is flexibility in the type of complex map used, as well as in the complex mapping parameters they contain, and guidelines for optimising the choices of both are provided in [3]. The major disadvantage of the method is the loss of the eigenfunction. The approximate solution is now represented by function values along a complex contour and not on the real axis. Thus complex maps are useful only on eigenproblems where the eigenvalue is of primary interest. If the eigenfunction is required, it must be computed by alternative methods.

In this study, we investigate once again the effectiveness of complex maps in matrix methods (finite difference and pseudospectral) for solving hydrodynamic stability problems. In particular, we wish to improve upon the results of previous work with unmapped methods for the barotropic vortex model [12]. The work of Boyd [3] serves as our starting point and we concentrate on the complex maps of polynomial type described in that paper. A more general form of the cubic map is proposed, and methods for optimizing the parameters in the maps are considered. In the case of a single critical latitude, an analytic result for determining the optimum map is presented.

The complex maps are described in Section 2, beginning with the quadratic map before generalizing to cubic maps. Calculation of the eigenfunction is also discussed in that section. Section 3 discusses the problem of determining the best map for both finite difference and pseudospectral methods. The complex mapping matrix methods are applied to two test problems in Subsection 4.1 before being applied to the barotropic stability problem in Subsection 4.2. Section 5 contains a summary of the results.

2. THE COMPLEX MAP

Consider a general second-order linear ordinary differential eigenproblem

$$a_2(y)u''(y) + a_1(y)u'(y) + a_0(y)u(y) = 0, \tag{1}$$

subject to linear, homogeneous, possibly mixed boundary conditions

$$\alpha_A u(-1) + \beta_A u'(-1) = \alpha_B u(1) + \beta_B u'(1) = 0, \tag{2}$$

where the prime denotes differentiation with respect to y, the $a_i(y)$ are known functions of y and possibly the eigenvalue λ, and the α_A, α_B, β_A, β_B are known real constants. It has been assumed that the original interval has been appropriately transformed to $[-1, 1]$ (either by a linear transformation for a finite interval or an appropriate nonlinear transformation for a semi-infinite or infinite interval [18, 19]).

For the problems considered in this paper the differential equation (1) possesses at least one regular singular point, or critical latitude, at the real or complex points y_c defined by $a_2(y_c) = 0$. For inviscid hydrodynamic stability problems $a_2(y)$ is some positive power of $U(y) - c$, where $U(y)$ is the undisturbed basic flow and c is the wavespeed of the normal mode perturbation. Here the critical latitudes occur at those points where the wavespeeds of the perturbation and the basic flow match. For strong instability, with $\mathrm{Im}(c)$ large, the critical latitudes will have large imaginary parts, but for neutral stability calculations, where the problem is solved with $\mathrm{Im}(c) \to 0$, the critical latitudes will have small or zero imaginary parts and thus lie close to or on the computational domain.

The nature of the singularities may be determined by an examination of the Frobenious expansion around the critical latitudes. For the problems considered in this paper the solutions behave as either $(y - y_c)\ln(y - y_c)$ or $(y - y_c)^{1/2 \pm i\mu}$, where $\mu \in \mathbf{R}$. Although both solutions are continuous their derivatives are discontinuous at the critical latitudes. For each critical latitude a branch cut passing to infinity, but not crossing the computational domain, must be specified. For real critical latitudes, physical arguments in [4] show that the cut must pass to infinity in the upper half-plane when $a_2'(y_c) > 0$ and in the lower half-plane when $a_2'(y_c) < 0$.

Pseudospectral methods, being global methods, are particularly sensitive to critical latitudes and their rate of convergence is limited by the singularity that is nearest in the sense of lying on the smallest ellipse in the complex plane with foci at $(\pm 1, 0)$ [22]. For critical latitudes on or near the interval $[-1, 1]$ spectral accuracy is lost and convergence becomes very slow. Finite difference methods are more robust in that their order of convergence, although much lower than for pseudospectral methods, is not affected by critical latitudes until they are within a very small distance from $[-1, 1]$, as noted in Boyd [3].

In either case, a complex map may be useful in restoring the accuracy lost due to the presence of critical latitudes. Under the independent variable transformation $y = f(x)$ with f a complex function and $x \in [-1, 1]$ the new (real) independent variable, (1) and (2) become

$$\frac{a_2[f(x)]}{(f'(x))^2}u''(x) + \left\{\frac{a_1[f(x)]}{f'(x)} - \frac{f''(x)a_2[f(x)]}{(f'(x))^3}\right\}u'(x) + a_0[f(x)]u(x) = 0 \tag{3}$$

and

$$\alpha_A u(-1) + \frac{\beta_A}{f'(-1)}u'(-1) = \alpha_B u(1) + \frac{\beta_B}{f'(1)}u'(1) = 0. \tag{4}$$

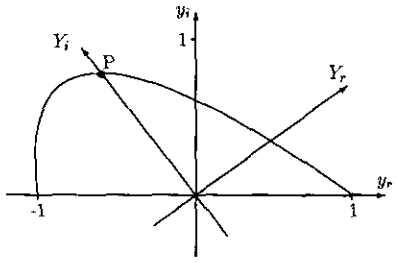

FIG. 1. Example of a contour produced by the complex quadratic map (5). The turning point of the curve is at P. Its axis is parallel to the rotated coordinate axis Y_i.

The map f must be chosen so that $f(-1) = -1$ and $f(1) = 1$ implying that the new path still passes through the boundary points, but as x varies from -1 to 1 a contour in the complex y-plane is followed. This contour can then be chosen to avoid the critical latitudes, but in doing so it must not cross any branch cuts. In addition, the maps themselves should not contain singularities and the curves generated should be both smooth and simple. The maps considered in this paper are polynomials of degree 2 or 3, but a generalization to higher degree is also suggested.

2.1. *Quadratic Mapping*

The quadratic map in Boyd [3], to which much of that paper was devoted, can be written as

$$y = f(x) = x - P(x^2 - 1), \tag{5}$$

where $P \in \mathbf{C}$ is the mapping parameter. (Here we have replaced Boyd's parameter Δ with P, where $P = i\Delta$ and $i = \sqrt{-1}$). This is the most general quadratic map with fixed points at $(\pm 1, 0)$. If y_r and y_i are the real and imaginary parts of y, the shape of the contour in the complex y-plane determined by this map is a parametric curve defined by

$$y_r = x - P_r(x^2 - 1)$$
$$y_i = -P_i(x^2 - 1)$$

as the parameter x varies from -1 to 1. Although this curve is a parabola it is in a nonstandard form since its axis is not vertical (see Fig. 1). The equation for this parabola can be written as

$$y_r^2 - 2\alpha y_r y_i + \alpha^2 y_i^2 + \frac{1}{P_i} y_i - 1 = 0,$$

where $\alpha = P_r/P_i$. Under the orthogonal rotation

$$\begin{bmatrix} Y_r \\ Y_i \end{bmatrix} = (1 + \alpha^2)^{-1/2} \begin{bmatrix} 1 & -\alpha \\ \alpha & 1 \end{bmatrix} \begin{bmatrix} y_r \\ y_i \end{bmatrix} \tag{6}$$

this becomes

$$Y_i = \alpha Y_r - P_i(1 + \alpha^2)^{1/2}[(1 + \alpha^2)Y_r^2 - 1]$$

which is a parabola with axis parallel to the Y_i axis. The turning point of this parabola (in the original coordinates) is determined from $dy_i/dy_r = 0$ and occurs at $(y_r, y_i) = (P_r, P_i) = P$. Figure 1 illustrates this curve for the quadratic complex map (5). Notice how the curve may bend back behind the endpoint in order to avoid the critical latitude. This also indicates that the curves generated by complex maps should be viewed as parametric relations.

2.2. *Cubic Mapping*

The second map described by Boyd is the cubic

$$y = f(x) = x - Qx(x^2 - 1), \tag{7}$$

where $Q \in \mathbf{C}$ is the mapping parameter. (Again we have replaced Δ, now with $Q = i\Delta$). The curve generated by this map is a cubic under the orthogonal transformation (6) with Q replacing P. This curve is forced to pass through the origin and, hence, is suitable only for the case of two symmetrically placed real critical latitudes. The most general cubic map with fixed points at $(\pm 1, 0)$ has four degrees of freedom and it is preferable to consider maps of this class when dealing with two arbitrary critical latitudes. This general cubic map can be defined by

$$y = f(x) = x - (P + Qx)(x^2 - 1), \tag{8}$$

where $P, Q \in \mathbf{C}$ are the mapping parameters. This map includes both the Boyd cubic ($P = 0$) and the quadratic ($Q = 0$). Examples of possible curves generated by (8) are given in Fig. 2. The last example illustrates a situation where a loop may occur. Since the curves generated should be as smooth and simple as possible these loops (as well as cusps) are unwanted features of a complex map. The first task then is to identify conditions on the parameters P and Q which eliminate these possible curves being generated by the map (8).

Equation (8) can then be separated into real and imaginary parts,

$$y_r = x - (P_r + Q_r x)(x^2 - 1)$$
$$y_i = -(P_i + Q_i x)(x^2 - 1),$$

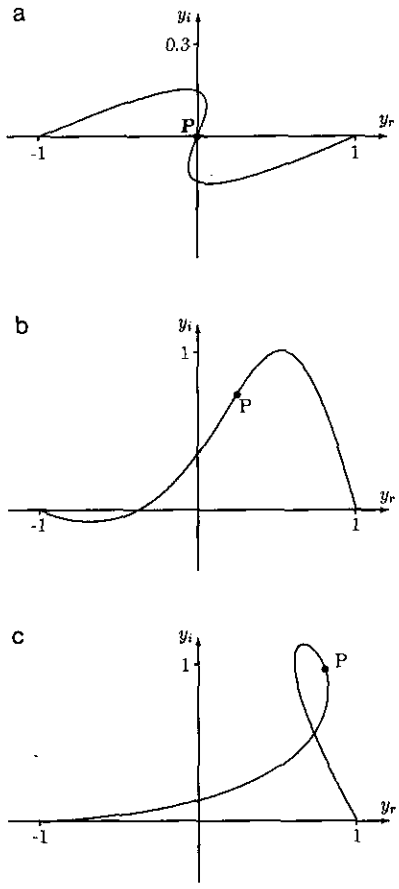

FIG. 2. Examples of contours produced by the complex cubic map (8): (a) $P = 0$, $Q = -1.3 - 0.4i$ (a Boyd cubic); (b) $P = 0.25 + 0.75i$, $Q = -0.25 + 1.2i$; (c) $P = 0.8 + 1.0i$, $Q = -1.3 + 0.9i$ (a cubic with a loop).

so that

$$y_r = x + \left(\frac{P_r + Q_r x}{P_i + Q_i x}\right) y_i.$$

The parameter x can be eliminated if the restriction

$$P_r Q_i = P_i Q_r \tag{9}$$

is imposed, giving

$$\frac{P_r + Q_r x}{P_i + Q_i x} = \alpha, \tag{10}$$

where α is a real constant. The result is the cubic equation

$$y_i = -[P_i + Q_i(y_r - \alpha y_i)][(y_r - \alpha y_i)^2 - 1].$$

Under the orthogonal transformation (6) this equation becomes

$$Y_i = \alpha Y_r - [P_i(1 + \alpha^2)^{1/2} + Q_i(1 + \alpha^2)Y_r][(1 + \alpha^2)Y_r^2 - 1], \tag{11}$$

so the generalized cubic map cannot contain any cusps or loops.

The conditions (9) and (10) can be enforced explicitly by the substitutions

$$P = \beta_0(\alpha + i), \quad Q = \beta_1(\alpha + i),$$

where $\alpha, \beta_0, \beta_1 \in \mathbf{R}$, are the new mapping parameters. Equation (8) then becomes a three-parameter family of cubics

$$y = f(x) = x - (\alpha + i)(\beta_0 + \beta_1 x)(x^2 - 1), \tag{12}$$

which includes the Boyd cubic and quadratic maps ($\beta_0 = 0$ and $\beta_1 = 0$, respectively). Figure 3 illustrates the curve for the cubic complex map (12).

The contour determined by the mapping (8) without the restriction (9) is actually a Bezier cubic. These curves are used when computer aided design is employed in numerically controlled machinery. In these fields, also, it is important to avoid loops and cusps. In a recent paper Stone and DeRose [23] characterize the Bezier cubics, the result being a diagram which describes regions of parameter space containing cusps, loops, or inflection points. The cubic map (8) can be analysed in the same way and it was found that the three-parameter family (12) corresponds to the so-called one inflection point line of the characterization diagram (their Fig. 5). Stone and DeRose note that this is a degenerate case which occurs "when the parametric cubic becomes the graph of a cubic function." This is confirmed by (11). Some generality is lost with the cubic map (12) as there are other cubic maps that are free of cusps and loops. However, there appears to be no other simple constraint like (9) which guarantees such maps are produced.

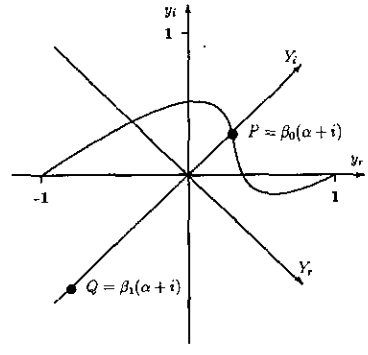

FIG. 3. Example of a contour produced by the three parameter family of cubic maps (12). With respect to the rotated coordinates (Y_r, Y_i) the curve is a cubic in one variable.

The three-parameter map also suggests a natural generalization to higher degree. Suppose we are given $n + 1$ real critical latitudes in $[-1, 1]$ with successive branch cuts in alternating directions. The most general complex polynomial map of degree $n + 2$ with fixed points at $(\pm 1, 0)$ is

$$y = f(x) = x - (P^{(0)} + P^{(1)}x + \cdots + P^{(n)}x^n)(x^2 - 1), \quad (13)$$

where $P^{(0)}, P^{(1)}, \ldots, P^{(n)} \in \mathbf{C}$. Consider the restriction of (13) to the $(n + 2)$ parameter family of maps for which all the $P^{(j)}$ lie on a common line through the origin. If $\alpha = P_r^{(j)}/P_i^{(j)} \in \mathbf{R}$ is the common ratio, and $\beta_j = P_i^{(j)}$, then this family of complex maps is given by

$$y = f(x) = x - (\alpha + i)(\beta_0 + \beta_1 x + \cdots + \beta_n x^n)(x^2 - 1). \quad (14)$$

The parameters can be chosen so that the interior zeros of y_i are positioned between successive critical latitudes. It is easy to verify that (14) generates a polynomial curve under the orthogonal transformation (6), therefore avoiding both cusps and loops.

2.3. *Eigenfunction Calculation*

Although the complex map enables accurate computation of the eigenvalues of a problem, this is at the expense of the eigenfunctions. The solution along the real y-axis cannot be inferred from the solution found along the complex contour. This is no problem, provided the eigenvalue is of primary interest. In many hydrodynamic stability problems the neutral curve or growth rate curve is often the characteristic sought and this involves only the eigenvalues.

However, if the eigenfunction is required, this too can be calculated, but at the expense of solving an additional problem. There are several methods for doing this, as suggested in [3]. First, if the critical latitudes are complex an unmapped pseudospectral or finite difference method can be used, but at higher resolution. The expense of the increased resolution is offset by the fact that one is now solving an ordinary boundary value problem whose operation count is much lower than that of the original eigenproblem. If the critical latitude is real, such as in neutral curve calculations and the Sturm–Liouville problems of the fourth kind, then a finite difference method, combined with a mapping producing a small deviation around the critical latitude, could be used. However, fine resolution would be needed to traverse the singular region. Another technique is to combine a Runge–Kutta method with a Frobenious expansion around the critical latitudes. This can be used for both real and complex critical latitudes. We used this technique to compute the eigenfunctions for the examples in Section 4. It is easy to implement and provides an independent check on the eigenvalues found by the complex mapping matrix methods.

3. SELECTING THE PARAMETERS

Having adopted the complex map (12), the problem now becomes the choice of the three parameters α, β_0, and β_1. The best choice, from an approximation viewpoint, would be that which maximizes the rate of convergence of the underlying matrix method. As such it will be different for the finite difference and pseudospectral methods. In the case of a single arbitrary critical latitude y_c, the optimum is a quadratic map ($\beta_1 = 0$). This case is treated separately, as an analytic result can be obtained.

3.1. *Single Critical Latitude*

Finite difference methods are more robust than pseudospectral methods in that the complex map is required only when the critical latitude is less than ah away from $[-1, 1]$, where h is the smallest allowable gridsize and a is the order of the method. This is because of the local nature and low order of the approximation. The critical latitudes of the transformed problem (3) will occur at $x_c = f^{-1}(y_c)$. This inverse function is multivalued, in general, and for the quadratic map is given by

$$x_c = x_\pm = f^{-1}(y_c) = [1 \pm (1 - 4Py_c + 4P^2)^{1/2}]/(2P) \quad (15)$$

Hence, the single critical latitude y_c is mapped into two critical latitudes $x_\pm$ for the transformed problem. Thus if a map is required for the finite difference method it must be chosen so that both x_+ and x_- are at least ah away from $[-1, 1]$. We look for the path satisfying this condition that is closest to the real interval and that does not cross the branch cut of the original critical latitude. This is achieved simply by placing P, the turning point of the curve, directly above or below the critical latitude a distance ah away. The branch cut direction determines the side on which to place P. This results in simple formulae for α and β_0.

Pseudospectral methods offer much higher orders of convergence but are more sensitive to critical latitudes. The coefficients a_n of a Chebyshev series of a function $u(x)$ have the asymptotic form $a_n \sim (\text{const})n^{-k}\delta^{-n}$ (see [18]). The dominant part in this expression is δ^{-n}, where δ is geometrically equal to the sum of the semi-major and semi-minor axes of the smallest ellipse with foci at $(\pm 1, 0)$ that passes through one of the transformed critical latitudes x_+ or x_-. The value of δ is given by

$$\delta = \min_{x_c = x_\pm} \{\max[|x_c + (x_c^2 - 1)^{1/2}|, |x_c - (x_c^2 - 1)^{1/2}|]\}, \quad (16)$$

and the contour should be chosen so as to maximize this value. A table of numerically calculated optimal δ values and the corresponding mapping parameters was provided in [3] for the case of a real critical latitude. There it was assumed that the branch cut passes to infinity in the upper half-plane. The method was simply to evaluate δ through (15) and (16) for various mapping parameters and the given critical latitude y_c and to

pick the best one. However, the following theorem shows it is possible to determine the optimal P analytically, not only for a real critical latitude but for any arbitrary complex one.

THEOREM 1. *Let $y_c \in \mathbf{C}$ be an arbitrary critical latitude and define δ as in* (16) *and $x_\pm$ as in* (15). *Then the quadratic complex map* (5) *that maximizes δ has*

$$P = (y_c \pm (y_c^2 - 1)^{1/2})/2 \tag{17}$$

and

$$\delta = \max\left\{\left|\frac{1 + (1 - 4P^2)^{1/2}}{2P}\right|, \left|\frac{1 - (1 - 4P^2)^{1/2}}{2P}\right|\right\}, \tag{18}$$

where the sign in (17) *is chosen to avoid the branch cut associated with y_c.*

Proof. The proof is in two stages. The first stage is to show that, for δ to be a maximum, x_+ and x_- must lie on the same ellipse with foci at $(\pm 1, 0)$. The second stage is to show that x_+ and x_- must be equal. This means that y_c is the branch point of f^{-1} and the result follows.

To prove the first part, introduce

$$\gamma(x) = x \pm (x^2 - 1)^{1/2} \tag{19}$$

with the sign chosen to maximize $|\gamma(x)|$. (With this choice, $\gamma(x)$ will be well defined and analytic everywhere, except on the interval $[-1, 1]$.) Define the real-valued function $\delta(x)$ to be $|\gamma(x)|$, and $\gamma_\pm$ and $\delta_\pm$ to be $\gamma(x_\pm)$ and $\delta(x_\pm)$, respectively. Then $\delta = \min\{\delta_+, \delta_-\}$ is the quantity to be maximized. Since $x_\pm$ is given by (15), $\gamma_\pm$ is a function of P that is analytic everywhere, except where $x_\pm$ is singular and where $x_\pm \in [-1, 1]$. Now if P changes by ΔP, $\delta_\pm^2$ changes by

$$\Delta(\delta_\pm^2) \simeq \overline{\gamma}_\pm \frac{d\gamma_\pm}{dP}\Delta P + \gamma_\pm \frac{d\overline{\gamma}_\pm}{d\overline{P}}\Delta\overline{P}$$

$$= 2\,\mathrm{Re}(\overline{\gamma}_\pm \frac{d\gamma_\pm}{dP}\Delta P).$$

If for some P, δ_+ and δ_- are not equal, and $\delta_- < \delta_+$, say, ΔP can be chosen so that $\Delta(\delta_-^2) > 0$. Thus δ_- can be increased, possibly at the expense of reducing δ_+. (The modulus of ΔP may need to be chosen to be small enough to prevent δ_+ from becoming smaller than δ_-.) The overall effect will be an increase in δ, and so δ could not be a maximum for that value of P. Thus, for the optimum value of P, δ_+ and δ_- must be equal.

Suppose now that δ_+ and δ_- are equal and so x_+ and x_- lie on the same ellipse with foci at $(\pm 1, 0)$. We wish to choose ΔP so that both δ_+ and δ_- will increase. This will mean that ΔP must satisfy $\mathrm{Re}(\Delta P\overline{\gamma}_+ d\gamma_+/dP) > 0$ and $\mathrm{Re}(\Delta P\overline{\gamma}_- d\gamma_-/dP) > 0$. Such a ΔP can always be found, unless

$$\overline{\gamma}_+ \frac{d\gamma_+}{dP} = -a\overline{\gamma}_- \frac{d\gamma_-}{dP}, \tag{20}$$

where a is a positive real number. This condition must be satisfied if P maximizes δ. Since $\overline{\gamma}_+\gamma_+ = \overline{\gamma}_-\gamma_-$, (20) can be written as

$$\frac{1}{\gamma_+}\frac{d\gamma_+}{dP} = -a\frac{1}{\gamma_-}\frac{d\gamma_-}{dP}. \tag{21}$$

Now the relationship

$$P = \frac{x_\pm - y_c}{x_\pm^2 - 1}, \tag{22}$$

which follows from (5), can be used to show that

$$\frac{dx_\pm}{dP} = -\frac{(x_\pm^2 - 1)^2}{x_\pm^2 - 2y_c x_\pm + 1}.$$

This equation, together with the relationship $\gamma^{-1}d\gamma/dx = \pm(x^2 - 1)^{-1/2}$, can be used to simplify each term in (21). After some algebra we obtain

$$\frac{1}{\gamma_\pm}\frac{d\gamma_\pm}{dP} = \pm\frac{(x_\pm^2 - 1)^{1/2}}{(1 - 4Py_c + 4P^2)^{1/2}}. \tag{23}$$

(Note that the choice of sign in (23) depends on the sign chosen in (19), as well as the choice of x_+ or x_-.) Equation (21) now implies $(x_+^2 - 1)^{1/2} = \pm a(x_-^2 - 1)^{1/2}$ and so $x_+^2 - 1 = a^2(x_-^2 - 1)$. Equation (22) can now be used to show that

$$x_+ - y_c = a^2(x_- - y_c). \tag{24}$$

If we recall that x_+ and x_- were assumed to lie on the same ellipse with foci at $(\pm 1, 0)$, (24) implies that either $x_+ = x_-$ or y_c must lie outside the ellipse. This second possibility would contradict the requirement that P maximize δ and so $x_+ = x_-$. ∎

For the case of $y_c \in \mathbf{R}$, with the branch cut in the upper half-plane, the optimal P lies on the semi-circle $P_r^2 + P_i^2 = (\frac{1}{2})^2$ in the lower half-plane. The transformed critical latitude $x_c = x_- = x_+$ will lie on the unit semi-circle in the upper half-plane.

TABLE I

Optimal Quadratic Map for a Single Real Critical Latitude

	Analytic			Boyd		
y_c	P_r	P_i	δ	P_r	P_i	δ
0.0	0.000	−0.500	2.414	0.0	−0.500	2.41
0.1	0.050	−0.497	2.410	0.050	−0.500	2.40
0.2	0.100	−0.490	2.397	0.100	−0.490	2.39
0.3	0.150	−0.477	2.375	0.150	−0.480	2.34
0.4	0.200	−0.458	2.342	0.200	−0.460	2.31
0.5	0.250	−0.433	2.297	0.260	−0.450	2.26
0.6	0.300	−0.400	2.236	0.300	−0.400	2.23
0.7	0.350	−0.357	2.154	0.360	−0.370	2.11
0.8	0.400	−0.300	2.040	0.400	−0.300	2.04
0.85	0.425	−0.263	1.961	0.430	−0.265	1.94
0.90	0.450	−0.218	1.859	0.455	−0.220	1.84
0.95	0.475	−0.156	1.704	0.480	−0.150	1.69
0.98	0.490	−0.0995	1.541	0.492	−0.100	1.54
0.99	0.495	−0.0705	1.444	0.499	−0.0712	1.43
0.998	0.499	−0.0316	1.283	0.500	−0.0312	1.27

Note. The analytic values given by (17) and (18) are presented in columns 1–4. Boyd's numerical results are given in columns 5–7.

These results are presented in columns 1–4 of Table I. For comparison, the results of Boyd (his Table I) are repeated in columns 5–7, in terms of the mapping parameter P.

3.2. *Several Critical Latitudes*

When there is more than one critical latitude, no analytic result is generally available and a numerical optimization of the mapping parameters of the complex map is required. We look specifically at the use of the cubic map in problems with two critical latitudes $y_c^{(1)}$ and $y_c^{(2)}$. The extension to multiple critical latitudes is straightforward.

With the pseudospectral method, the problem is to choose α, β_0, and β_1 so as to maximize δ, subject to the constraint that the contour does not cross a branch cut. In this case, however, the points $f^{-1}(y_c)$ are now the roots of a cubic equation and so there may be up to six transformed critical latitudes. This problem can be converted to an unconstrained minimization problem. The objective function was chosen to be $F = -\delta$, and a penalty, M, was added for any curve that crossed a branch cut. The IMSL routine DBCONF was used for the minimization. With some distributions of multiple critical latitudes, a quadratic map may still be optimal. This is the case for the barotropic vortex model to be considered later. In this case the optimization procedure starting with the cubic (12) correctly produced the quadratic curve.

For the finite difference method, the map must again be chosen so the transformed critical latitudes remain at least ah away from the interval $[-1, 1]$, where a is the order of the method and h is the grid spacing. This condition does not result in explicit formulae for the parameters α, β_0, and β_1 and so the problem was once again converted to a minimization. The maximum displacement of the contour from $[-1, 1]$ was minimized subject to the constraints that $|\mathrm{Im}\{f^{-1}(y_c^{(j)})\}| > ah$ for each of the transformed critical latitudes, and that the contour does not cross a branch cut. Penalties proportional to $[ah - |\mathrm{Im}\{f^{-1}(y_c^{(j)})\}|]$ were added if $|\mathrm{Im}\{f^{-1}(y_c^{(j)})\}| < ah$, and a penalty M was added if the contour crossed a branch cut.

4. NUMERICAL CALCULATIONS

The problems considered here include two test problems (with singularities on or near the real axis) and the barotropic vortex model examined by [10, 12]. These problems are all second-order, linear differential eigenproblems. The methods used were the pseudospectral method (PSM) and the second-order and fourth-order finite difference methods (FDM2 and FDM4, respectively). The implementation of FDM2 was as described in [12], but with a second-order approximation being used for the derivative term in the boundary condition. Similarly, for FDM4, a fourth-order expression for the derivative was used at the boundary. The pseudospectral method (referred to as the discrete ordinate method in [12]) was implemented by collocating at Chebyshev–Lobatto nodes. The eigenfunction was expanded in a finite sum of Lagrange polynomials, resulting in the function values at the nodes becoming the coefficients of the expansion. The methods were coded in Fortran 77 and run on a Unix workstation employing double precision arithmetic. The generalized matrix eigenproblems were solved using the IMSL routine DGVLCG.

4.1. *Test Problems*

The so-called Sturm–Liouville problems of the fourth kind are such that both the differential equation and the eigenfunctions are singular at some real interior point of the domain. In order to investigate problems of this type, Boyd [4] considers a related problem where the singularity is just off the real axis and then looks at the limiting case as the singularity approaches the axis. The most important consequence of this is that the eigenvalues and eigenfunctions need no longer be real. Other authors (see, for example, [24]) have adopted a different approach and interpreted such problems as being defined on spaces that are direct sums of intervals on the real line. This approach leads to quite different conclusions concerning the eigenvalues and eigenfunctions. In this paper we follow the interpretation of Boyd. We present first an example with a double pole at the origin in order to illustrate an application of the quadratic map. The differential equation chosen is

$$y^2u''(y) + (1 - \lambda y^2)u(y) = 0 \tag{25}$$

subject to

$$u(-1) = u(1) = 0, \tag{26}$$

The direction of the branch cut from the origin cannot be deduced from the conditions $a_2'(y_c) < 0$ or $a_2'(y_c) > 0$ since $a_2'(y) = 2y$ is zero there. We choose, arbitrarily, the direction in the upper half-plane. Equation (25) is a transformed Bessel equation and the solution satisfying (26) is

$$u(y) = By^{1/2}J_{-i\sqrt{3}/2}(i\lambda^{1/2}y),$$

where λ is a solution of

$$J_{-i\sqrt{3}/2}(i\lambda^{1/2}) = 0.$$

The eigenvalues occur in conjugate pairs and can be ordered in increasing modulus. The algebraic package Mathematica [25] was used to calculate the first two eigenvalues with positive imaginary part. To 16 decimal places these are

$$\lambda_1 = -4.6405397088235620 + 6.471082787454876i \quad (27)$$

$$\lambda_2 = -29.3538288396719996 + 14.9678408170587427i. \quad (28)$$

Since this problem has only a single critical latitude, Theorem 1 gives $P_{\text{OPT}} = -0.5i$ and $\delta = 2.414$ for the pseudospectral method. Figure 4a compares the relative error in λ_1 and λ_2 found with the pseudospectral method with $N = 32$ for a range of quadratic maps by varying P_i but keeping $P_r = 0$. For λ_2, it is evident that $P = -0.5i$ is optimal. For λ_1, the minimum is less well defined. The most likely reason for this is the influence of round off errors at these high accuracies. Similar graphs for $N = 24$ and $N = 16$ (not presented) both show sharp minima in the relative error of λ_1 at $P = -0.5i$ and so confirm this view.

The relative errors obtained with the optimal map are plotted for various values of N in Fig. 4b. The unmapped method was totally inadequate here and returned only real eigenvalues, regardless of the number of nodes used. Because of this, the results obtained for the map with $P = -0.1i$ are presented for comparison with the results from the optimal map. The relative error for the optimum map decreases sharply with increasing N until around $N \sim 32$, and then it increases slowly. This increase is most likely due to roundoff error and supports the statements concerning the minimum for λ_1 in Fig. 4a. Also, as suggested by Theorem 1 and Fig. 4a, convergence with this map is significantly faster. Both λ_1 and λ_2 are determined to an error of less than 10^{-12} with just 32 nodes. With the nonoptimal map an error of around 5×10^{-3} had been achieved with the same resolution.

Like their pseudospectral counterparts, the unmapped finite difference methods also failed to resolve the singularity at the origin. However, the optimally mapped finite difference methods did show their expected second- and fourth-order convergence with N for both λ_1 and λ_2. Here $P_{\text{OPT}} = -ahi$, where a is the order of the method and $h = 2/(N-1)$ is the grid spacing. Figure 5 shows the dependence of the relative errors in λ_1 and λ_2 on the location of P for each of the finite difference methods with $N = 32$.

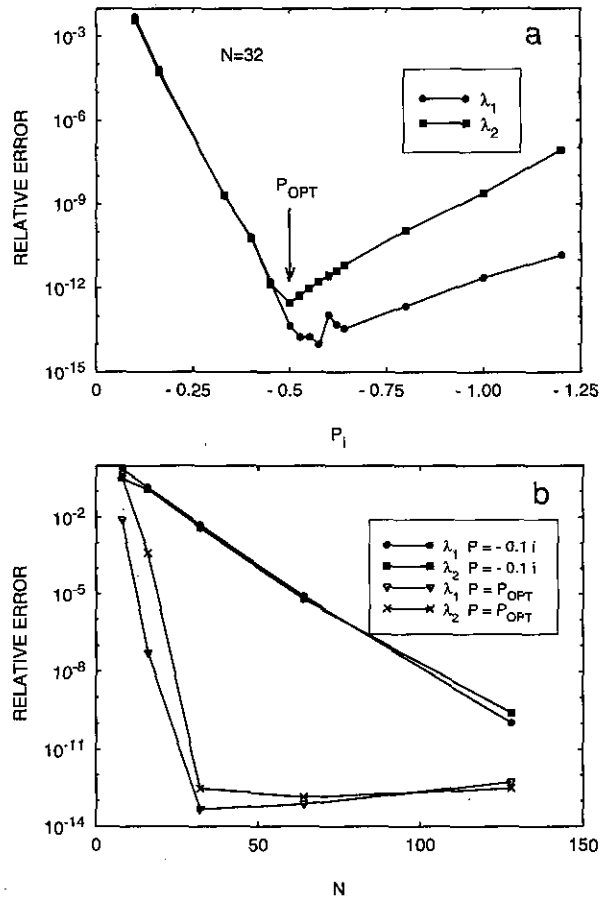

FIG. 4. Relative errors (in logscale) in λ_1 and λ_2 for (25) and (26), using the quadratic map pseudospectral method: (a) variation with location of $P = iP_i$ for $N = 32$; (b) convergence with N for $P = P_{\text{OPT}} = -0.5i$ and $P = -0.1i$.

Unlike the pseudospectral method these methods are relatively insensitive to P_i for $P_i < -ah$, which is a result of the local nature of the finite difference approximation. Surprisingly they also appear insensitive in the approximate range $-ah/2 > P_i > -ah$. As a result, the location of the minimum is quite broad. This indicates that for finite difference methods a nonoptimal map will not degrade the method as much as it would in a pseudospectral method. This robustness of finite difference methods is useful, but one cannot look past the extremely high accuracy of the mapped pseudospectral method for this problem.

To test the cubic map (12) the following problem was solved:

$$u''(y) + [(y - y_c^{(1)})^{-1}(y - y_c^{(2)})^{-1} - \lambda]\, u(y) = 0, \quad (29)$$

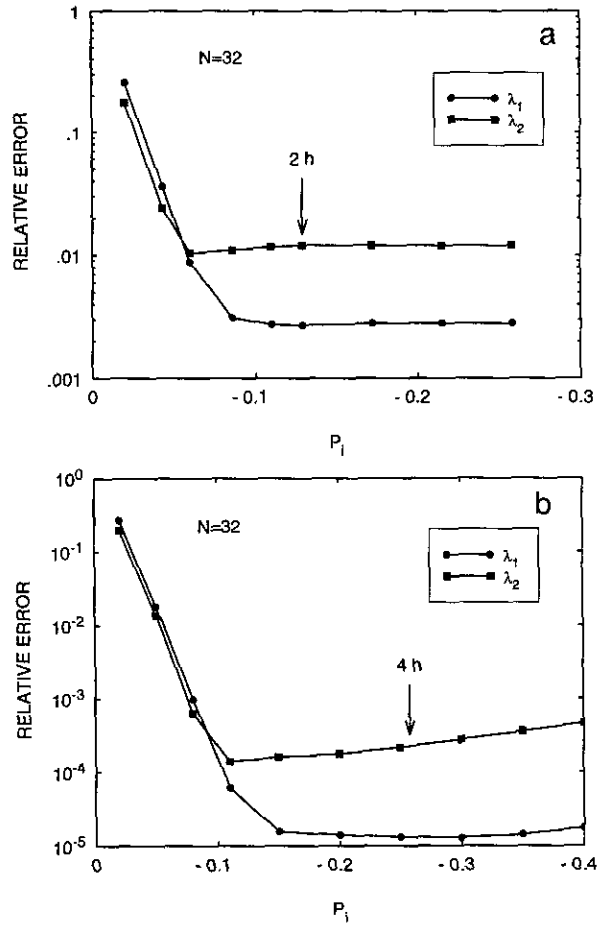

FIG. 5. Quadratic map finite difference method with varying $P = iP_i$ for $N = 32$. Plotted are the relative errors (in logscale) in λ_1 and λ_2 for (25) and (26) using (a) the second-order method; (b) the fourth-order method.

subject to

$$u(-1) = u(1) = 0, \tag{30}$$

where $y_c^{(1)} = -0.25 - 0.1i$ and $y_c^{(2)} = 0.5 + 0.1i$ are the two complex critical latitudes with branch cuts in opposite directions. The lack of symmetry in the location of the poles excludes Boyd's cubic ($\beta_0 = 0$) from being optimal and thus necessitates the use of the cubic map (12). The absence of real singularities enables a comparison between the optimally mapped and unmapped methods, unlike the situation in solving (25) and (26). It also eliminates the need for a complex mapping in the finite difference methods, once a certain resolution is achieved and, thus, only the pseudospectral method will be considered here.

Equation (29) is related to the spheroidal wave equation. However, this does not appear to help in determining the eigenvalues of (29) and (30). Consequently, we take as our "true" eigenvalues the results from the optimally mapped pseudospectral method at intermediate resolution. Results from higher resolution are likely to be more affected by roundoff error. Ordered as before, we find

$$\lambda_1 = -3.802534765803 + 4.795914298127i \tag{31}$$

$$\lambda_2 = -8.773291569069 + 4.995230738019i, \tag{32}$$

where we have used the $N = 100$ result for λ_1 and the $N = 80$ result for λ_2.

The parameters for the optimal cubic map for this problem were found numerically to be

$$\alpha = 0.6752, \quad \beta_0 = 0.1208, \quad \beta_1 = -0.5347, \tag{33}$$

yielding a δ value of 1.636, whilst the unmapped pseudospectral method offers only $\delta = 1.109$. Figure 6 displays the convergence of the pseudospectral method for both of these cases for the first two eigenvalues of (29) and (30). The results for the cubic mapping are just as impressive as for the quadratic map. The first two eigenvalues are resolved to a relative error of less than 5×10^{-13} with just 40 nodes under the optimal mapping. The unmapped pseudospectral method could only return relative errors of 7×10^{-4} and 4×10^{-4} for λ_1 and λ_2, respectively, for the same resolution.

4.2. *Barotropic Stability Problem*

Barotropic models have become popular in recent years for describing tropical cyclone dynamics. Many numerical stability analyses have been carried out for representative velocity profiles; see, for example, [10, 12]. In [12] the pseudospectral and finite difference methods were compared and it was found that the pseudospectral method did not perform as well as expected. This was finally attributed to the presence of critical latitudes and their proximity to the real axis. The differential equation

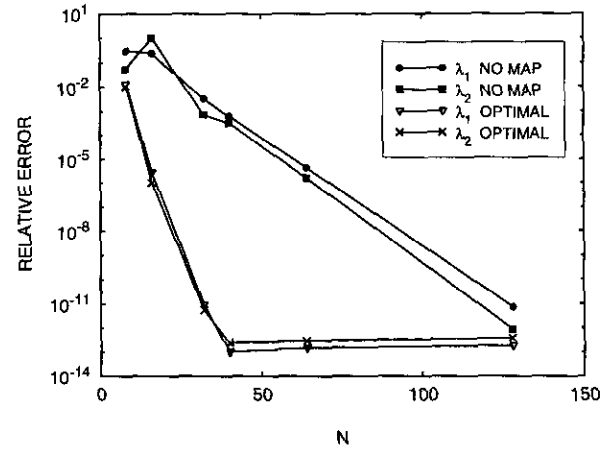

FIG. 6. Convergence of the optimal cubic and the unmapped pseudospectral method for (29) and (30). Plotted are the relative errors (in logscale) as functions of N.

governing the linear stability of normal mode perturbations is

$$[\Omega(r) - c]\left[u''(r) + \frac{u'(r)}{r} - \frac{m^2}{r^2}u(r)\right] - \frac{\Gamma'(r)}{r}u(r) = 0, \quad (34)$$

subject to

$$u(0) = \lim_{r\to\infty} u(r) = 0, \quad (35)$$

where c, the wavespeed, is the eigenvalue. Here $\Omega(r)$ is the basic angular velocity, $\Gamma(r) = r\Omega'(r) + 2\Omega(r)$ is the vorticity, m is the tangential wavenumber of the perturbation, and $u(r)$ is the radial amplitude of the perturbation to the streamfunction. Physically valid solutions to (34) correspond to an integer wavenumber m; however, the quantities of interest in this problem are often the values of the frequency $\omega_r = m\ \mathrm{Re}(c)$, and the growth rate $\omega_i = m\ \mathrm{Im}(c)$ as functions of the wavenumber treated continuously. We restrict the values of m to those with $\mathrm{Im}(c) > 0$ as the flow is then unstable. In particular, we seek the eigenvalue with the largest imaginary part as this yields the maximum growth rate.

For the profiles examined in [12], the critical latitudes are determined by $r_c = \Omega^{-1}(c)$, where Ω^{-1} is multi-valued. Furthermore, the locations of the critical latitudes for a given wavenumber are not known *a priori*, as these depend on the eigenvalue c. If the problem is to be solved for a range of wavenumbers, this difficulty is handled by a continuation approach. That is, the critical latitudes for the previous wavenumber are used to determine the complex map for the current wavenumber. For the first wavenumber, the unmapped method was used. Provided successive wavenumbers are close enough and the first critical latitude is not too close to the real axis, this procedure gives satisfactory results.

As it stands, the domain for this problem is semi-infinite. For the profiles examined in [12] it was found that domain truncation to $[0, R]$ with $R = 10$ was preferable to an algebraic or exponential map. This is due to the rapid decay of both $\Omega(r)$ and $\Gamma'(r)$ at large r. An appropriate outer boundary condition was then constructed from the asymptotic form of $u(r)$.

Five velocity profiles were examined in [12] but here only two will be considered. These are the Chan and Williams (CW) profile $\Omega(r) = \exp[-r]$ and the narrow Smith (SN) profile

$$\Omega(r) = \frac{1 + 3l(\mu r^2)^2}{[1 + \mu r^2 + l(\mu r^2)^3]^2},$$

where the shape parameters have values $l = 0.2032$ and $\mu = 0.5218$.

Results from [12] indicate an unstable wavenumber range of $1.0 < m < 1.41$ for the CW profile and $1.0 < m < 2.44$ for the SN profile. Thus the CW profile is stable to all physical wavenumbers (integer m), whereas the SN profile has one unstable mode at $m = 2$. Also from these results the critical latitudes for both profiles can be calculated. For the CW profile there are an infinite number given by $r_c = -\mathrm{Log}(c) + 2n\pi i$, $n \in \mathbf{Z}$, but only those with $|n| \leq 1$ will be influential. The critical latitudes for the SN profile are solutions of a sixth degree polynomial for μr^2 but only those with $\mathrm{Re}(r_c) \geq 0$ will be important.

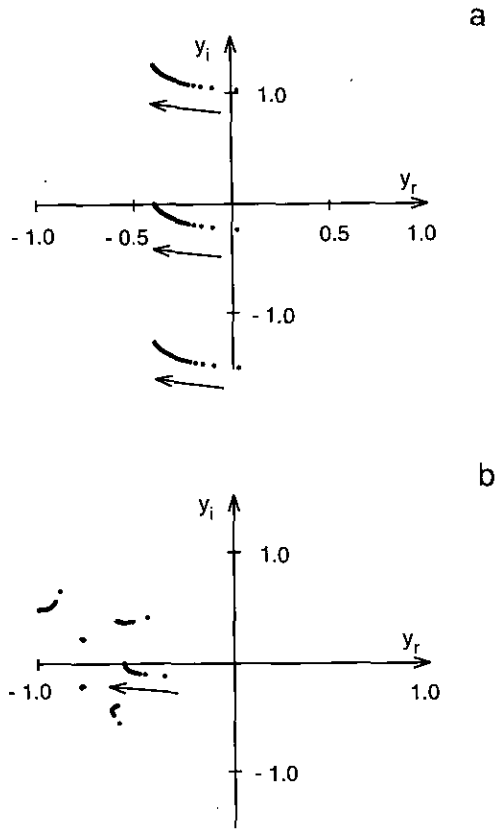

FIG. 7. Location of the critical latitudes in the complex y-plane where $y_c = (2r_c - R)/R$. The arrows denote the direction of increasing wavenumber: (a) CW profile. $1.0 < m < 1.41$; (b) SN profile $1.0 < m < 2.44$.

Figure 7 shows how these critical latitudes vary with m. In this figure, the linear rescaling $y_c = (2r_c - R)/R$ has been applied to convert the computational domain to $[-1, 1]$. The arrows denote the direction the critical latitudes move as m increases. Thus the critical latitudes approach the real axis at the upper limit of unstable wavenumbers for both profiles. Notice also that two of the SN profile's critical latitudes are nearly fixed. The branch cut for each critical latitude is chosen to pass to infinity vertically upwards or downwards if the critical latitude is in the upper or lower half-plane, respectively.

As discussed in Subsection 4.1, the absence of real critical latitudes eliminates the need for a complex mapped finite difference method, so attention will again be focused on the pseudospectral method. The distribution of the critical latitudes for both profiles suggests a quadratic map will be sufficient. This

was confirmed by numerical optimization of δ using the cubic map (12). The result was that $\beta_1 = 0$ which yields the quadratic map as expected.

Initial results were not as impressive as for the test problems. This was due to the regular singularity of (34) at the origin ($r = 0$), where $u(r) \sim r^m$. For noninteger m the solution exhibits discontinuous derivatives at the origin. As this is an endpoint, no complex mapping will help. However, this singularity is removable by a simple dependent variable transformation such as $v(r) = r^{1-m}u(r)$ so that $v(r) \sim r$ as $r \to 0$. In the results which follow, this transformation has been applied to (34) before the complex map.

For the barotropic stability problem there are no closed form solutions, so once again the eigenvalues were compared with those obtained from the optimally mapped pseudospectral method at intermediate resolution. To compare the convergence of the unmapped and mapped pseudospectral methods for the CW profile we fixed the wavenumber at $m = 1.2$ as in [10]. The "true" nondimensional frequency and growth rate were found to be

$$\omega_r = 0.043754707539, \quad \omega_i = 0.019703854041. \quad (36)$$

Because there is more than one critical latitude, a numerical optimization of the quadratic map is required. The optimal map has $P = -0.1589 + 0.3746i$ which yields a δ value of 1.855, whilst the unmapped pseudospectral method has only $\delta = 1.095$. Figure 8a displays the convergence of both methods by plotting the logarithm of the relative errors in both the frequency and growth rate for various N. Once again the results for the mapped method are impressive.

For higher wavenumber values, the critical latitude approaches the real axis and the convergence of the unmapped method becomes even slower, whilst the mapped method maintains the high convergence obtained for $m = 1.2$. In fact, over the entire unstable wavenumber range $1.0 < m < 1.41$, the mapped method calculated the frequencies and growth rates with relative errors no worse than 7×10^{-10} and 2×10^{-9}, respectively, using just 32 nodes. With the same resolution, the unmapped method calculated the frequencies to a relative error of no more than 4×10^{-2}. However, the calculated growth rates were significantly worse. A relative error of more than 1% was returned for $m \geq 1.23$ and relative errors of more than 10% were returned for $m \geq 1.31$. This is a direct result of the critical latitude approaching the real axis near the upper limit of unstable wavenumbers.

For the SN profile the critical latitudes are generally much closer to the real axis than those of the CW profile and, consequently, the increase in δ resulting from using the complex quadratic map will not be as great. We first considered the same wavenumber as for the CW profile, $m = 1.2$. Here we found $\delta = 1.100$ for the unmapped pseudospectral method and $\delta = 1.263$ for the optimal quadratic map. Hence the mapped method shows only a modest improvement over the unmapped method.

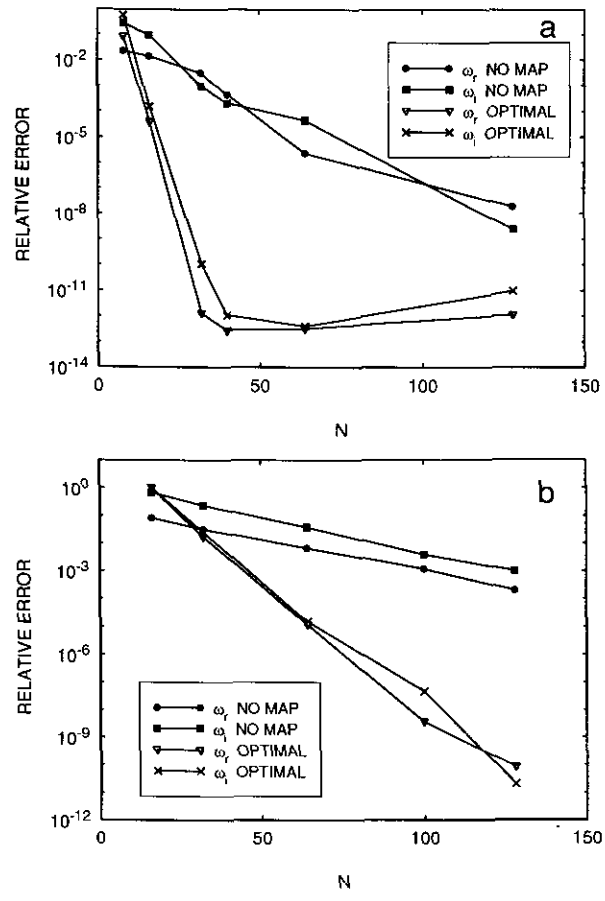

FIG. 8. Convergence of the optimal quadratic and the unmapped pseudospectral method to the frequency (ω_r) and growth rate (ω_i) of the barotropic stability problem: (a) CW profile $m = 1.2$; (b) SN profile $m = 2$.

The benefit of the complex mapping in this case is more evident at higher wavenumbers. For example, for the integer wavenumber $m = 2$, the "true" nondimensional frequency and growth rate are

$$\omega_r = 0.181589254818, \quad \omega_i = 0.041421414230. \quad (37)$$

Again, a numerical optimization of δ is required which results in the optimal quadratic map with $P = -0.1955 + 0.1459i$ and $\delta = 1.214$, whilst the unmapped method has only $\delta = 1.029$.

The convergence of both methods for $m = 2$ is illustrated in Fig. 8b, where again the logarithm of the relative errors in both the frequency and growth rate are plotted as functions of N. In contrast to Fig. 8a convergence of both methods is slower, but the complex mapping is still far more accurate. The difference between the methods is more stark when solving the problem near the upper limit of unstable wavenumbers. In this region the unmapped method has little hope of resolving the singularity.

5. SUMMARY

In this paper, we have re-examined the polynomial complex maps of Boyd [3] and produced a more general cubic mapping which includes the quadratic map. A natural generalization to a higher degree was also explicitly given. An analytic result for the optimal quadratic complex map, given a single arbitrary critical latitude, was produced, but a more general analytic result appears unlikely.

Both the quadratic and cubic complex maps were tested on model problems using both finite difference and pseudospectral methods. Both methods benefited from the use of the complex maps, particularly the pseudospectral method which is more sensitive to the critical latitudes. This sensitivity is offset by its ability to produce highly accurate solutions. The barotropic vortex model was then solved with the quadratic mapped pseudospectral method for two velocity profiles. Again, vast improvements over the unmapped method were observed, particularly at the upper limit of unstable wavenumbers.

Our results for the barotropic vortex model (see Fig. 8) clearly show that the complex map can still be of considerable benefit even when the critical latitude is not on the real axis. This is in contrast to the suggestion in [9] that a complex mapping may not be needed in such cases. Even at maximum growth rates (occurring at $m = 1.14$ for the CW profile) the critical latitudes may still be significantly close to the real axis to warrant a complex mapping.

The complex maps demonstrated in this paper are easy to implement and give remarkable gains in accuracy. This suggests to us that they should always be considered when solving problems containing critical latitudes, including the large class generated by inviscid hydrodynamic stability calculations. We believe the complex mapped pseudospectral methods will be strong competitors to existing techniques.

ACKNOWLEDGMENTS

We thank Professor R. J. Hosking for his interest and support. One of us (A.W.G) acknowledges the financial support received from an Australian Postgraduate Research Award. This project was also supported by a James Cook University Merit Research Grant.

REFERENCES

1. P. G. Drazin and L. N. Howard, *Adv. Appl. Mech.* **9,** 1 (1966).
2. K. Stewartson, *IMA J. Appl. Math.* **27,** 133 (1981).
3. J. P. Boyd, *J. Comput. Phys.* **57,** 454 (1985).
4. J. P. Boyd, *J. Math. Phys.* **22**(8), 1575 (1981).
5. J. A. Adam, *Phys. Rep.* **142**(5), 263 (1986).
6. J. P. Boyd, *J. Atmos. Sci.* **39,** 770 (1982).
7. M. R. Osborne, *SIAM J. Appl. Math.* **15**(3), 539 (1967).
8. J. P. Boyd, *Mon. Weather Rev.* **106,** 1192 (1978).
9. W. W. W. Liou and P. J. Morris, *Int. J. Numer. Methods Fluids* **15,** 1407 (1992).
10. H. C. Weber and R. K. Smith, *Geophys. Astrophys. Fluid Dyn.* **70,** 1 (1993).
11. C. Canuto, M. Y. Hussaini, A. Quarteroni, and T. A. Zang, *Spectral Methods in Fluid Dynamics* (Springer-Verlag, New York, 1988), p. 31.
12. A. W. Gill, G. E. Sneddon, and R. J. Hosking, *Geophys. Astrophys. Fluid Dyn.* **72,** 57 (1993).
13. J. P. Boyd and Z. D. Christidis, *Geophys. Res. Lett.* **9,** 769 (1982).
14. J. P. Boyd and Z. D. Christidis, "Instability on the Equatorial Beta-Plane," in *Hydrodynamics of the Equatorial Ocean,* edited by J. Nihoul (Elsevier, Amsterdam, 1983), p. 339.
15. J. P. Boyd and Z. D. Christidis, *Dyn. Atmos. Oceans* **11,** 139 (1987).
16. G. E. Sneddon and I. B. Whittingham, *J. Phys. B: At. Mol. Phys.* **23,** 2227S (1990).
17. C. E. Grosch and S. A. Orszag, *J. Comput. Phys.* **25,** 273 (1977).
18. J. P. Boyd, *J. Comput. Phys.* **69,** 112 (1987).
19. J. P. Boyd, *J. Comput. Phys.* **70,** 63 (1987).
20. J. M. Augenbaum, in *Proceedings, 2nd IMACS Symposium on Computational Acoustics, Princeton* (Elsevier–North Holland, Amsterdam, 1990).
21. A. Bayliss, D. Gottlieb, B. J. Matkowsky, and M. Minkoff, *J. Comput. Phys.* **81,** 421 (1989).
22. A. Solomonoff and E. Turkel, *J. Comput. Phys.* **81,** 239 (1989).
23. M. C. Stone and T. D. DeRose, *ACM Trans. Graphics* **8**(3), 147 (1989).
24. W. N. Everitt, J. Gunson, and A. Zettl, *Angew. Math. Phys.* **38,** 813 (1987).
25. S. Wolfram, *Mathematica, A System for Doing Mathematics by Computer* (Addison–Wesley, New York, 1988).